Chemical Engineering Journal 466 (2023) 143152

Contents lists available at ScienceDirect

Chemical Engineering Journal

journal homepage: www.elsevier.com/locate/cej

Engineering brain-derived neurotrophic factor mRNA delivery for the treatment of Alzheimer's disease

Haoyuan Li [a], Yan Cao [b], Jingjing Ye [c], Zhipeng Yang [d], Qimingxing Chen [b], Xiaoqin Liu [e], Bohan Zhang [f], Jingwen Qiao [d], Qisheng Tang [a], Huiying Yang [g], Jianfeng Li [b], Zhifeng Shi [a,*], Ying Mao [a,*]

[a] Department of Neurosurgery, Huashan Hospital of Fudan University, National Center for Neurological Disorders, Shanghai Key Laboratory of Brain Function Restoration and Neural Regeneration, Neurosurgical Institute of Fudan University, Shanghai 200040, China
[b] Gene Editing Center, School of Life Science and Technology, ShanghaiTech University, Shanghai 201210, China
[c] Centre for Discovery Brain Sciences, University of Edinburgh, Edinburgh EH89LD, United Kingdom
[d] Academy for Engineering & Technology, Fudan University, Shanghai 200433, China
[e] Department of Pharmacy, Shanghai Chest Hospital, Shanghai 200040, China
[f] School of Physical Science and Technology, ShanghaiTech University, Shanghai 201210, China
[g] Department of Pharmacy, Huashan Hospital of Fudan University, Shanghai 200040, China

ARTICLE INFO

Keywords:
Brain-derived neurotrophic factor
mRNA delivery
Poly (β amino esters)
3′UTR modification
Alzheimer's disease

ABSTRACT

Brain-derived neurotrophic factor (BDNF) has a long history in the treatment neurodegenerative of diseases. However, this therapy has limitations in exogenous protein safety, including side effects like neuropathic pain and seizures. Moreover, there are currently no positive clinical trial results using BDNF-based gene therapy. Given this, new methods of delivering BDNF are urgently needed. Here, we report an engineering BDNF mRNA-based therapy in a murine model of Alzheimer's disease (AD). Two poly (β amino esters) polymers (PBAE) were synthesized, which achieved mRNA delivery to brain and spinal cord efficiently following catheter ventricle pumping. To confer stability and RNase resistance, the secondary structure of the mRNA was engineering using AI algorithms. Further mRNA modification was done on 3′ untranslated region (3′UTR), which was added with neuron-specific miRNA targeting sequence to avoid BDNF protein expression in neuron. This allowed reduced neuronal overexcitation and seizures. And BDNF protein was sustained released from astrocytes to maintain surrounding neural function. The engineering mRNA was delivered into the brain ventricle and translated into astrocytes to significantly improve the memory of AD mice. Given the mRNA modifications presented here, it would de-target delivery to specific cell types and has therapeutic potential for the treatment of neurological diseases.

1. Introduction

Brain-derived neurotrophic factor (BDNF) has a long history of use, particularly in therapeutic applications for central nervous system diseases. For instance, a dozen years ago, BDNF protein was infused using a programmed pump in patients with Alzheimer's Disease (AD). However, the exogenous protein-induced neuropathic pain occurred in all three participants of the study. Ultimately, this led to a halt of using BDNF protein in clinical treatment [1,2]. After this initial attempt, AAV2-based nerve growth factor gene therapy was used to treat AD. The phase I results were promising [3], but unfortunately failed in phase II [4]. This may be attributed to two factors: the immune system response triggered by AAV and a restricted delivery volume for achieving promising results. Additionally, gene therapy remains some barriers to its use, after repeat injection, the virus will be cleared by specific neutralization antibody [5]. And the virus can integrate into the genome with potential carcinogenic risk [6]. Thus, new technology should continue to be tested. Messenger RNA (mRNA) drugs showed strong potential in allowing high protein expression with less side effects [7,8]. Given this, mRNA based on non-viral delivery could be an alternative approach for neurotrophic factors-based therapeutics.

An aging central nervous system is vulnerable to a host of problems,

* Corresponding authors.
E-mail addresses: shizhifeng@fudan.edu.cn (Z. Shi), maoying@fudan.edu.cn (Y. Mao).

https://doi.org/10.1016/j.cej.2023.143152
Received 2 February 2023; Received in revised form 28 March 2023; Accepted 21 April 2023
Available online 23 April 2023

including epileptic seizure [9,10], inflammation [11], stroke [12,13] and tumors [14]. In a *trans*-genetic murine brain model, BDNF protein overexpression resulted in epileptic seizures [15]. In addition, high serum levels of BDNF protein were highly related to both seizure occurrence and severity. This was revealed with samples from 260 patients who were experiencing seizures [16]. Direct delivery of BDNF protein into the whole brain can cause seizures. On the contrary, BDNF gene specifically delivered to astrocytes instead of the whole brain by involving astrocyte-specific promoter (GFAP) does not result in seizure activity, and it has good therapeutic potential for use in AD by selective astrocyte delivery [17]. As for mRNA-mediated delivery, this approach has been successfully used to target the liver, lung, and spleen [18–21]. Targeting specific cells may remain challenging if using material modifications alone. However, when 3′UTR sequences of mRNA were modified with cell-specific miRNA target sequences, the mRNA only translated in the certain cell types [22]. Cell type-specific miRNA could be identified using high-throughput sequencing. After that, mRNA achieved cell-specific transcription by adding miRNA target sequences. This pattern of highly accurate delivery to specific cell types would unlock previous limitations and lower the side effects of treatment.

The instability of mRNA remains a challenge for its clinical applications. Past work has shown that mRNA secondary structures are formed by base pairing and contribute to protein expression [23]. Unpaired RNA sequences form loop structures, including multiloops, internal loops, hairpin loops, and bulge loops [24]. These loop structures increase the instability of mRNA, as they are more easily broken by RNase. This is due to lack of hydrogen bonds and their concurrent protection [24]. By optimizing synonymous codons, the mRNA secondary structures would change based on changing base-pairing. This could potentially lead to improved stability. The development of artificial intelligence (AI) accelerated the Covid-19 mRNA vaccine development, which can be approved by FDA within a year. The Moderna used AI to design the mRNA sequences, and it increased the mRNA generation quantity from 30 per month to 1000 per month. Pfizer also applied the AI algorithm to whole process of the vaccine development from sequencing design to manufacturing and clinical trials. However, those AI algorithms need supercomputing capacity, which is hard to access for research groups. Another AI algorithms, Linear Design, for mRNA secondary structure can achieve similar results with more stable mRNA and higher protein expression[25]. Thus, this user-friendly AI algorithm should be applied for modification of mRNA sequences.

A wide variety of materials in nucleic acid delivery have been developed, including poly(L-lysine) (PLL), Polyethylenimine (PEI), poly (β amino esters) (PBAE) and others [26–29]. PBAE offers three notable benefits in comparison to other materials. First, it has good biocompatibility and biodegradability. Second, PBAE exhibits good performance in transfecting various types of cells. Third, it can be easily to synthesize by Michael addition of amines to acrylates, so the large polymers library can be easily built [30].

Here, we designed two PBAE polymers as suitable for delivering mRNA directly to the central nervous system (CNS) by brain ventricle pumping. We then applied AI algorithm (Linear Design) to BDNF mRNA, for a more stable mRNA with higher transcription level. When used *in vivo* and as expected, mice experienced seizures as highly translation of BDNF mRNA. To solve the problem of neuronal over-activation, 3′UTR was modified with the neuron-specific miRNA-124 target sequence. In this way, engineering mRNA delivered into the neurons was degraded by miRNA. Whereas, mRNA was normally expressed in astrocytes. Finally, astrocytes released the BDNF to support neurons, thereby improving the memory of APP/PS1 double transgenic AD model mice (Fig. 1).

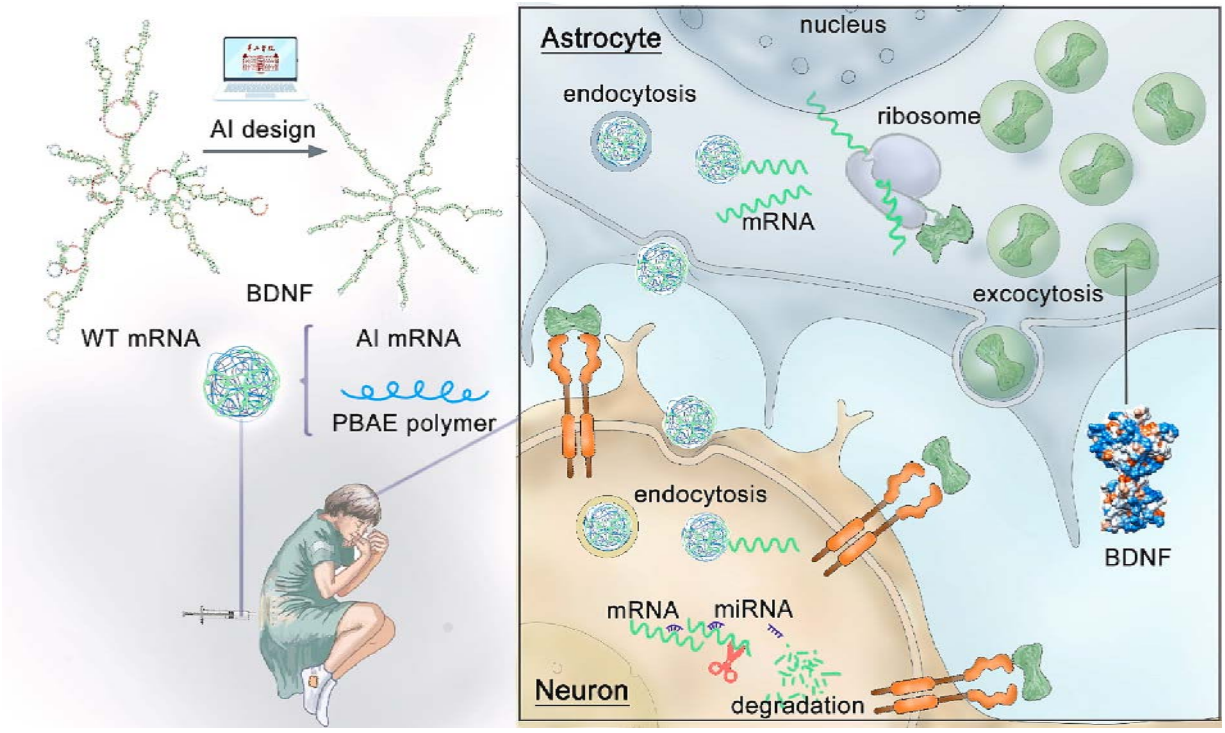

Fig. 1. Schematic illustrating the process of BDNF mRNA treatment for Alzheimer s Disease. The mRNA secondary structure was modified by AI algorithms to be more stable and more resistant to the RNase. After the addition of the PBAE, the nanoparticle was intrathecally injected and endocytosed into the cells. Due to negative side effects of BDNF administration (e.g., neuronal overexcitation and seizure), 3′UTR of the mRNA was modified by adding the neural-specific miRNA target sequence. When the mRNA was endocytosed into the neurons, the mRNA was degraded by miRNA. Importantly, the mRNA could still be translated into protein in the astrocytes. BDNF protein was then released and activated the receptor on the neurons to protect them from death.

2. Experimental section

2.1. mRNA synthesis

All mRNA sequences were designed based on previously published work [31]. Briefly, the CDS region was used instead of GFP or BDNF. The complementary sequence of miRNA-124, ggcattcaccgcgtgcctta, was added to the 3′UTR. The target mRNA sequence was added to the pBluescript II KS (–) plasmid (Genscript Biotech Corporation). For the linear model of DNA, the circle plasmid (10 ng) was amplified by Q5 high-fidelity DNA polymerase (New England Biolabs), and purified using the QIAquick PCR purification kit (QIAGEN). IVT mRNA synthesis was performed using HiScribe™ T7 ARCA mRNA Kit (with tailing) (New England Biolabs), with 1.25 mM Pseudo-UTP and 5mCTP (APExBIO) in the final step. After, mRNA was purified by Monarch RNA Cleanup Kits (New England Biolabs). The mRNA was quantified using Nanodrop 2000 (Thermo Fisher Scientific) and stored at 80 °C until later use. Luciferase and GFP mRNA were both purchased from APExBIO.

2.2. PBAE-111 and PBAE-211 synthesis

PBAE polymers were synthesized using a two-step process as previously described [28]. In the first step, the backbone was mixed using (B),1,4- butanediol diacrylate or ((propane-2,2-diylbis(4,1-phenylene)) bis(oxy)) bis(2-hydroxybutane-4,1-diyl) diacrylate and side chain (S), 4-amino-1-butanol in a 1.1:1 ratio. These two monomers were mixed and reacted under magnetic stirring at 90 °C for 24 h.

Acrylate-terminated polymers were dissolved in DMSO. Amine end capping reagent (E), pentane-1,3 diamine (molar ratio B: S: E = 1.1:1:10) were used to modify the polymer ending in THF under magnetic stirring at room temperature for 2 h. After being washed with diethyl ether, the polymers were lyophilized. Polymers were dissolved in DMSO at a concentration of 100 mg/mL and were stored at –20 °C until later use [32,33].

2.3. mRNA secondary structure modification

The mRNA secondary structure was modified based on the LinearDesign (Baidu Inc., https://rna.baidu.com/) and the CDS sequence obtained from NCBI (Reference Sequence: NM_001143805.1). The whole mRNA sequence or amino acid sequence was pasted in LinearDesign. The beam size ranged from 25 to 50 according to mRNA lowest minimum folding free energy change and secondary structures. Visualization and pairing prediction were based on LinearFold and LinearPartion (Baidu Inc.).

2.4. Nanoparticles formation

Polymers (PBAE-111, Mw = 7000 Da; PBAE-211, Mw = 6600 Da) were diluted in NaAC buffer (25 mM, pH = 5, Merk) from stored polymers solution (100 mg/mL); mRNA (200 ng/well in 96-well plates and 1 μg/well in 24-well plates) were also dissolved in the same quantity of NaAC buffer. The ratio between PBAE and mRNA was 80:1 (w/w) in PBAE-111 and 60:1 (w/w) in PBAE-211. Then, mRNA and PBAE were mixed by pipette and left undisturbed for 10 min. Before transfection to cells, 5× volume of buffer DMEM with 3 mg/mL BSA (Merk) was added to the mixture. As for mice brain injection, the mixture was then lyophilized to remove residual DMSO and stored at 80 °C until later use. The mixture was diluted with artificial cerebrospinal fluid (aCSF, Leagene Biotechnology) and 3 mg/mL BSA.

2.5. Physical and chemical properties of nanoparticles

The nanoparticles were made by vigorously mixing PBAE and mRNA in NaAC (25 mM) for 10 min, after which the mixture was diluted with pure water or PBS to determine the Zeta potential and particle size. The nanoparticles were characterized according to their diameters, surface charge, and morphology. Zeta potential and nano-size were measured by Zetasizer Nano (Malvern Instruments Ltd.) The morphology was determined using a transmission electron microscope (JEM-1400plus at 80 kV in Shanghai Tech University); 1H NMR was used for identification and was performed at Shanghai Tech University. Gel Permeation Chromatography of the polymer (GPC) was carried out in tetrahydrofuran (THF) utilizing a Malvern Viscotek TDAmax detection system. Samples were filtered over 0.22 μm filters before injection using a 1.0 mL/min flow rate. Molecular weights were determined by comparing to a linear polystyrene standard.

2.6. Cell culture

Mice primary neurons, primary astrocytes, 293T and neuron cell line SH-SY5Y were used in this study. For primary neurons, the cells were prepared following previously published protocols [34]. Briefly, pregnant ICR mice (day 15–17) were sacrificed and embryos were collected on ice in Hank's balance salt solution (HBSS; Gibco, Life Technologies). Two sterile injection syringes were used to dissociate the cortex from the encephalon. Brain tissue was dissected mechanically using a Pasteur pipet (Nest) into single cells and plated in 10% fetal bovine serum (Gibco, Life Technologies) in DMEM (Gibco, Life Technologies). After changing the culture medium by Neurobasal and 2% B27 (Gibco, Life Technologies), neurons were allowed to culture for additional two days and were then ready for experimental use. For primary astrocytes, cells were derived from P1 mice pups. The single-cell isolation technique was similar to the process used for neurons. After plating in 10% FBS DMEM for 4 h, the culture medium was changed. After 7 days, the T75 flask was centrifuged at 180 rpm for 2 h to remove microglia [10]. 293 T, SH-SY5Y cells were cultured in DMEM with 10% FBS. All cells were incubated at 37 °C in a humidified atmosphere of 5% CO_2 and 95% air.

2.7. Luciferase assay in vivo

ICR mice (4–6 weeks, Jiesijie) were housed in a temperature-controlled room on a 12 h light/12 h dark cycle with ad libitum access to food and water. The ethical approval was obtained from the Fudan University (2021–04-HSYY-SZF-001). Mice were anesthetized by isoflurane and a small hole (1 mm) was drilled in the cranial bone on the top of the injection site. mRNA (3 μg in 5 μL) was then slowly injected (0.5 μL/min) into the ventricle using a stereotaxic apparatus (X = 1 mm Y = -0.58 mm Z = 2.0 mm from bregma). The skin was carefully sutured and the mice were allowed to recover on a heating pad. After different amounts of time post-mRNA injection (8 h, 24 h, 36 h, and 48 h), mice received an intraperitoneal injection of D-luciferin potassium salt (Solarbio) to visualize in IVIS Lumina LT (PerkinElmer Inc.). The dose of D-luciferin was determined according to the mouse's individual weight (150 μg/g). Data were analyzed by Living Image® Analysis Software (PerkinElmer Inc.).

2.8. Agarose gel electrophoresis

Agarose powder (Biosharp) was mixed with 1× TAE (1% w/v). After heating, GelRed® Nucleic Acid Stain (Millipore) was added. The samples of mRNA or mRNA with PBAE were added to the gel with assistance of loading buffer (Thermo fisher). The gel was run at 120 V for 30 min and then visualized using UV (Tanon).

2.9. Immunostaining

Cells were fixed in 4% PFA, rinsed with PBS, and then permeabilized with 0.5% Triton X-100. Cells were then blocked with 3% serum (Boster) for 30 min and incubated with the following primary antibodies: anti-His tag (1:100, Proteintech), anti-BDNF (1:100, Boster), and anti-p-TrkB (1:100, Bioss) antibodies. Cells were then incubated with

secondary antibodies (1:100, Abbkine) for 1 h; nuclei were counterstained with DAPI (Boster). Images were obtained and analyzed using fluorescence microscopy (IX71; Olympus).

2.10. Cell transfection

Primary cells were plated (15,000 cells/well in 96-well plates or 50,000 cells/well in 24-well plates) or SH-SY5Y cells (8,000 cells/well in 96-well plates or 30,000 cells/well in 24-well plates) 2 days before use. The complex solution was then added into the wells (100 μL per well for 96 well-plates and 500 μL per well for 24 well-plates). Before changing the culture medium, the plates were incubated in the incubator for 3 h for neurons and 4 h for astrocytes. After 24 h, mRNA expression was determined.

2.11. Calcium imaging

Astrocytes grew for 2–3 d to cover the 35 mm dish. Flou-4 AM (Thermo fisher) was added at 3 μM (final concentration) and incubated for 30 min. After that, cells were washed with extracellular solution (Beyotime Biotechnology) and maintained at room temperature in the dark until acquisition. During visualization, 50 mM KCl was used to polarize the cell membrane potential and trigger vesicular release.

2.12. ELISA for BDNF

BDNF protein in the cells and culture medium was measured by a commercially available ELISA kit (Boster). Cells were lysed using RIPA lysis buffer (Beyotime). After centrifuging at 10,000 rpm for 5 min, the supernatant was collected and stored at 80 °C until later use. The culture medium was also stored at 80 °C until testing. The samples were processed following the manufacturer's instruction; the O.D. values were measured in a multi-well spectrophotometer at 450 nm.

2.13. Immunohistochemistry for brain tissue

Mice were deeply anesthetized and transcardially perfused with 4% PFA. Coronal sections of the hippocampus region were taken (10 μm thick). The following primary antibodies were used: anti-PSD-95 (1:200, Abcam), anti-pTrkB (1:100, Bioss), and anti-BDNF (1:100, Boster) antibodies. After rinsing with PBS, secondary antibodies (1:100, Abbkine) were applied and incubated for 60 min at room temperature. DAPI (Boster) was used as a nuclear counterstain. Fluorescence microscopy was used for all imaging.

2.14. Mouse surgery

APP/PS1 mice (9 months, Ailingfei Biotech) were housed as previously described. Fur was shaved and 75% ethanol was used to clean the skin on the surgical site. A 1.5 cm incision was made in the middle of the head and the tissues over the cranial bone were removed. The position for the injection was marked on the skull and a small hole (1 mm) was drilled. A microsyringe (32G) was used to first check the ventricle by observing the CSF overflow. The brain infusion catheter (DURECT Corporation) was then inserted into the ventricle and fixed by dental cement. The end of the tube was blocked by kwik sil (World Precision Instruments) to prevent bacterial infection in the brain. Importantly, the surface of the cement and tube was covered with picric acid to prevent being chewed by the mice.

2.15. Mouse mRNA injection

The PBAE-111 and mRNA lyophilized powder dissolved by aCSF (5 μL/mouse) with 3 mg/mL BSA before use. After mice were anesthetized by isoflurane, ethanol was used on the micro-syringe to sterilize it. The syringe was slowly inserted into the tube and the edge was sealed by parafilm. After, the injection speed was 1 μL/min, which was maintained for 2 min until the end of the injection. Finally, kwik sil was used to block the end of the tube to avoid bacterial infection. Picric acid was applied to the surface of the catheter to prevent being chewed by the mice.

2.16. Animal behavior tests

A month after mRNA injection, all behavioral tests were performed in the following order: Light/dark box, object location, and 8-arm mazes. Additional detail is provided below:

2.16.0.1. Light/dark box

The box contained two parts according to the intensity of light. The light in light box was 350 lx and in dark box was 2 lx. The two parts were connected by an aperture. Each mouse was released in the light box in the same corner. The test was run for a total of 6 min and the total time spent in each chamber was recorded. The mouse's movements were tracked, recorded, and analyzed using EthoVision XT (Noldus).

2.16.0.2. Object location test

Mice were released into an open field area (35 cm × 35 cm × 40 cm) and habituated to the new environment for 10 min. The next day, two patterns were placed on the open field arena. Each mouse was released into the arena and allowed to explore for 10 min. The spatial memory was tested after 24 h, with one pattern being moved to a new position. Mice were allowed to explore the open field area and their movements were tracked, recorded, and analyzed using EthoVision XT (Noldus).

2.16.0.3. 8-arm maze

The surrounding maze was marked with different graphs. The mice were fasted before being tested, with food being placed in 4 arms as a reward. Mice were trained to explore the maze and food for 10 min or food had been eaten in the first 5 days. The test was performed on the 6th day and the mouse's movements were tracked, recorded, and analyzed using EthoVision XT (Noldus).

2.17. Statistical analysis

Data were processed using Graphpad Prism 9. The student's *t* test was used to analyze the two groups; for three or more groups, ANOVA was used. Before ANOVA analysis, Brown-Forsythe test was used for homoscedastic and Bartlett's test was used for normal distribution, respectively. Tukey test was used as post hoc test to compare difference among groups. $*p$ 0.05; $**p$ 0.01; $***p$ 0.001; and $****p$ 0.0001.

3. Results

3.1. PBAE library scanning and identification

Cationic polymers PBAE are easy to synthesize and modified via Michael addition (Fig. 2a). After scanning the PBAE library [33], we identified both PBAE-111 and PBAE-211 as showing good potential for mRNA delivery to neural cells. PBAE-111 and 211 both have a common ending modification, pentane-1,3-diamine, and both polymers are linear; the differences exist in the backbone since PBAE-211 contains benzene. Mass spectra were identified, and these two polymers were synthesized as designed (Figs. S1 and S2).

To achieve mRNA delivery, protonated PBAE (in 25 mM NaAc) was electrostatically bound to anionic mRNA. The zeta potential of the mRNA was 34 ± 7.1 mV. After cationic PBAE-111 and 211 bindings, the zeta potential increased to 28.3±5.2 mV and 35.5±6.7 mV, respectively (Fig. 2b). The mRNA diameter size increased from 24.0 ±5.7 nm to 142.3±43.4 nm and PBAE-211 54.9±15.8 nm when bound to PBAE-111 and PBAE-211, respectively (Fig. 2c). Similarly, images from transmission electron microscopy (TEM) showed similar diameters

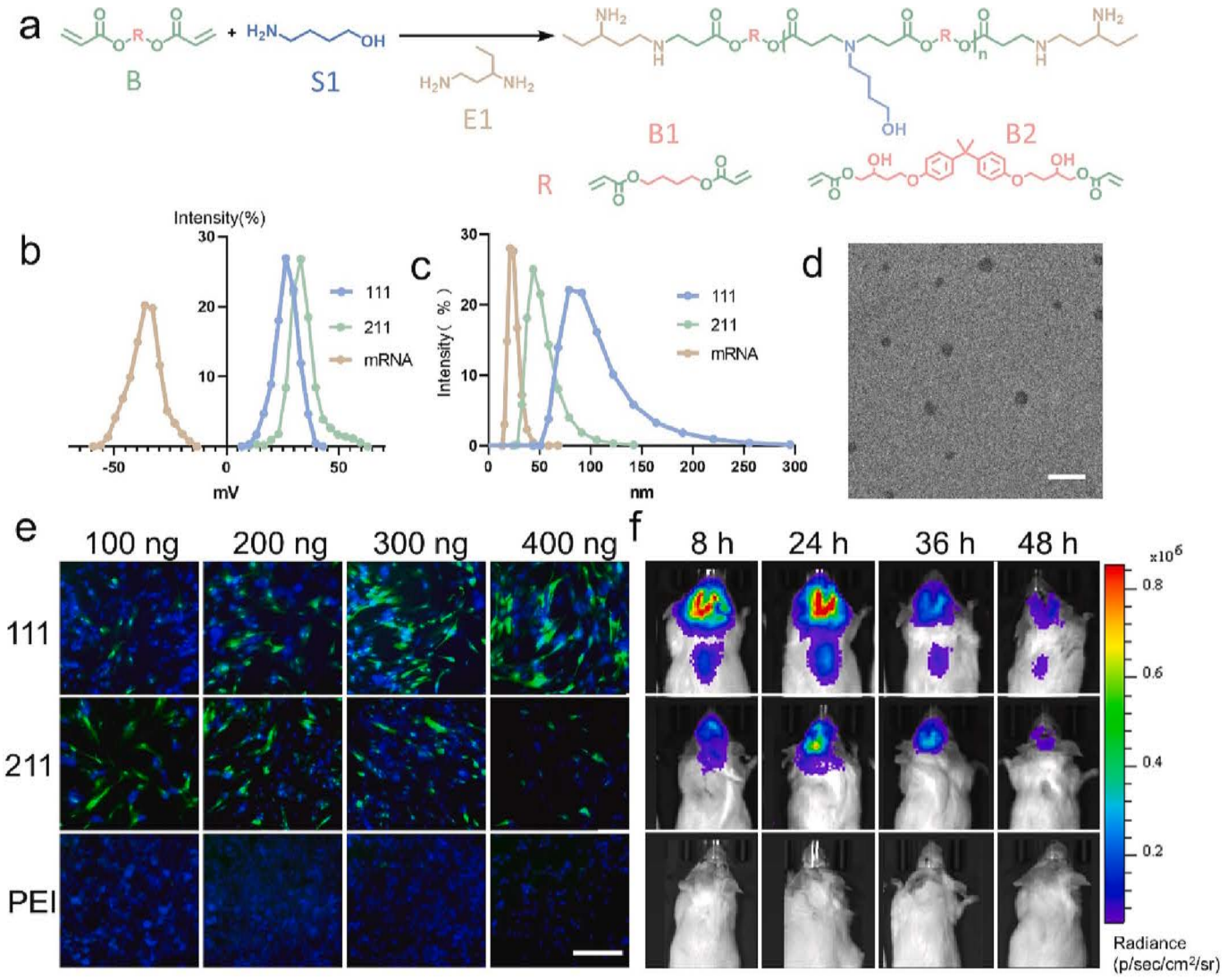

Fig. 2. Nanoparticle properties and transfection rates. (a) Synthetic process for PBAE B1S1E1 (111) and B2S1E1 (211). (b, c) Zeta potential (mV) and size diameters (nm) of mRNA and mRNA mixed with PBAE-111, 211. (d) Representative TEM image of nanoparticles formed by PBAE 111 and mRNA. Scale bar = 200 nm. (e) The transfection rate of PBAE 111, 211, and PEI with different doses of GFP mRNA in primary astrocytes. scale bar = 200 μm. (f) Biodistribution and transfection of luciferase mRNA by brain ventricle injection. B, Backbone; S, Side chain; E, Ending cap. (n = 3 biological repeats and 9 mice).

with laser diffraction particle sizes. These data also indicated the particles' morphology was circle and homogeneously distributed without accumulation (Fig. 2d).

To achieve nanoparticle distribution, the PBAE/mRNA complex was cultured with BSA to form protein corona (Fig. S3c). The zeta potential of the nanoparticle decreased to 3.53 ± 0.82 mV in PBAE-111 and 5.75 ± 0.58 mV in PBAE-211 (Fig. S3a and b). After protein corona formation, the complex became negative charge in surface and decrease the zeta potential variation in cerebrospinal fluid (CSF).

And the ratio between mRNA and PBAE higher than 1:60 can achieve high encapsulation efficiency (Fig. S5).

3.2. Transfection in vitro and in vivo

The PBAE transfection rate was tested in primary astrocytes and was compared with classic cationic polymers—PEI and commercial LNP, lipofectamine MessengerMax™. Generally, PBAE-111 demonstrated the highest GFP mRNA transfection efficiency across various concentrations (28.2±4.0% at 100 ng, 42.4±4.7% at 200 ng, 55.7±3.0% at 300 ng and 65.13±4.3% at 400 ng). Comparatively, PBAE-211 had high transfection efficiency at low mRNA dose (51.5±5.4% at 100 ng), but showed low transfection (31.7±0.19%) at higher mRNA dose (Fig. 2e). The PBAE-111 maintained good cell viability over a wide range of concentrations, with 99.3±4.0%, at 100 ng, 95.6±3.2% at 200 ng, 89.1±3.8% at 300 ng and 73.2±3.2% at 400 ng. However, PBAE-211 showed cytotoxic effects at dosages exceeding 300 ng (35.5±0.79% at 300 ng and 29.8±0.73% at 400 ng) (Fig. S3d). MessengerMax™ could achieve a transfection rate of 38% with both 300 ng and 400 ng (Fig. S4a). However, the classic cationic polymer PEI did not show any transfection capacity in primary cells (Fig. S4b).

The transfection rates of the cationic polymers were then tested *in vivo*. Luciferase (Luc) mRNA (3 μg) was mixed with PBAE-111, 211, and PEI and then slowly injected into the cerebral ventricle. Given the circulation of cerebrospinal fluid (CSF), Luc mRNA mixed PBAE-111 could translate protein throughout the entire CNS, including brain and spinal cord. The highest protein expression was $13.2\pm1.1\times10^6$ p/sec/cm^2/sr in 24 h and maintained for nearly 48 h. As for PBAE-211 delivery, mRNA was only expressed locally. The highest expression of Luc at 8 h after injection was $8.2\pm2.1\times10^6$ p/sec/cm^2/sr, and was similarly maintained for 48 h. As with cell transfection, PEI did not show Luc protein translation (Fig. 2f, Fig. S4c).

Collectively, these data showed two PBAE polymers that have good

potential for CNS delivery. More specifically, PBAE-111 demonstrated good transfection rate and wide distribution. Comparatively, PBAE-211 showed high transfection with low dose and was only ever locally distributed—even with cerebral ventricle injection.

3.3. mRNA secondary structure engineering

mRNA secondary structure was based on hydrogen bond between complementary base pairs. When changing nearly 18.4% of synonymous codons using AI algorithms, the structure of wild-type BDNF mRNA had decreased numbers of loops and unstable single strands (red) (Fig. 3a). The lowest minimum folding free energy change (MFE) increased from 218.5 kcal/mol to 483.7 kcal/mol (Fig. 3b). Bases were connected more locally instead of over longer distances (Fig. 3c), thus leading to reduced numbers of loop structures. Overall, this enhanced the stability of the mRNA. We then tested the mRNA stability in the presence of RNase at different temperatures. The whole process of gel preparation and use of EP tubes had no DEPC treatment to remove all RNase. Across a wide temperature range (20 °C to 37 °C), the AI-designed mRNA had greater stability than the wild type (Fig. 3d). Importantly, this AI-designed mRNA transcript had more targeted protein than wild type (3135±159 pg/mL vs. 2347±102 pg/mL) (Fig. 3e).

3.4. mRNA 3′UTR engineering

As expected, the seizure occurred in nearly 50% of mice after 8 h

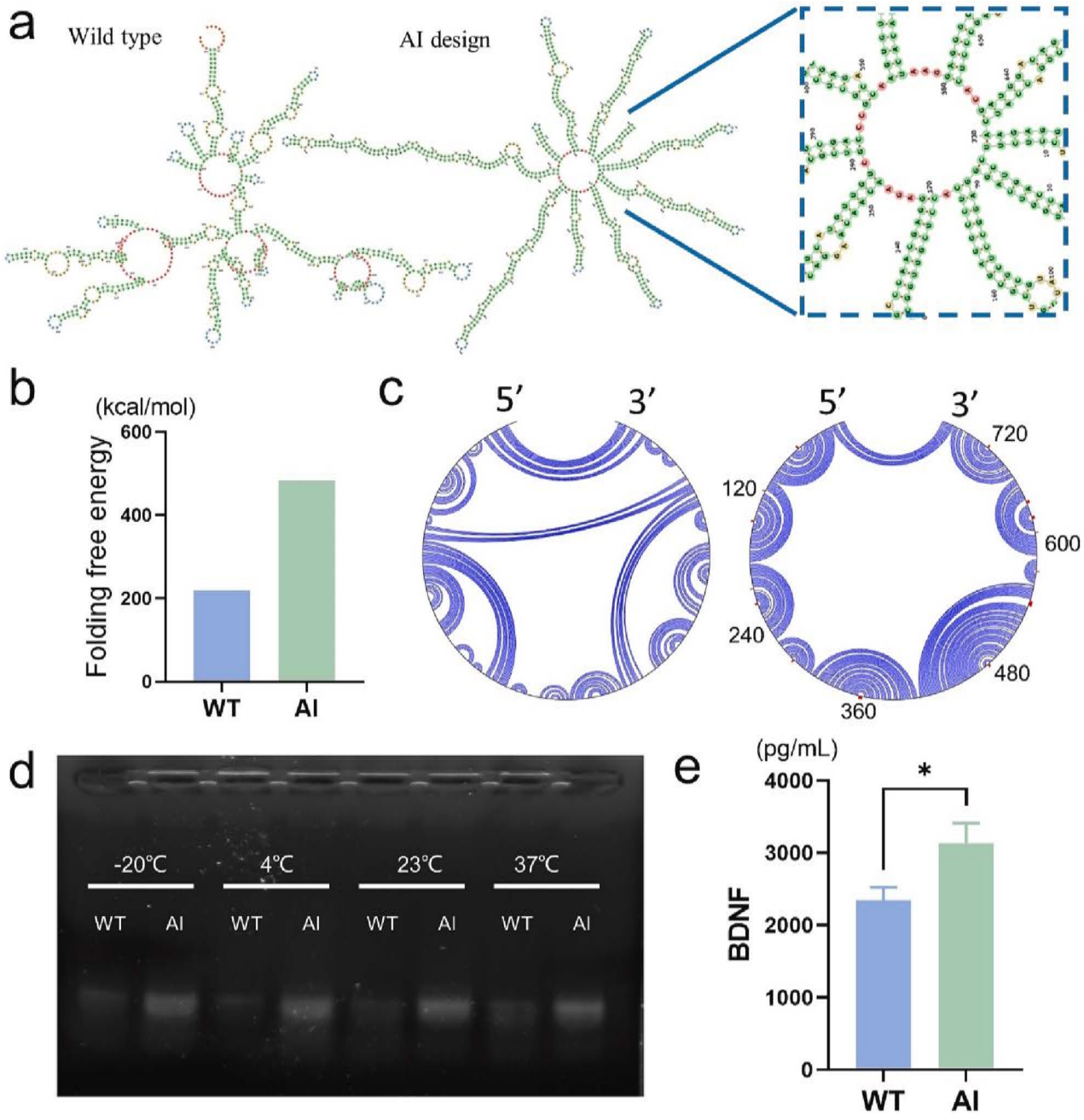

Fig. 3. Mrna engineering and modified by ai. (a). Secondary structures of mRNA. Paired base (stable, green), single base (unstable, red), between these two conditions (yellow). (b) Bar chart of lowest minimum folding free energy (MFE). (c) Chord diagram of mRNA base connection. AI contributed more base connections to be more stable and connected with closer bases to decrease loops. (d) The stability of mRNA in the presence of RNase determined using gel electrophoresis. (e) ELISA-quantified amount of BDNF protein expression. *p 0.05. (n = 3 biological repeats).

injection of the BDNF mRNA nanoparticle (Video 1). BDNF overexpression in neurons has previously been shown to result in neuronal overexcitation and seizure [16,35]. Given this, BDNF released locally by astrocytes was planned to avoid excessive neuronal excitability. Thus, we added a neural-specific miRNA-124 complementary sequence into the 3′UTR (Fig. 4a). During the mRNA delivery into the neurons, miRNA-124 would guide the Ago2 protein to degrade the mRNA (Fig. 4b and c). With the addition of 0–3 miRNA target regions, neurons exhibited GFP expression of 18.5±0.8% in 0 target region, 8.6±0.5% in 1 target region, 3.8±0.3% in 2 target region, and 0.1±0.06% in 3 target regions (Fig. 4d and e). As astrocytes lack miRNA-124, there was no obvious difference in GFP expression in the 0–3 target regions (37.2

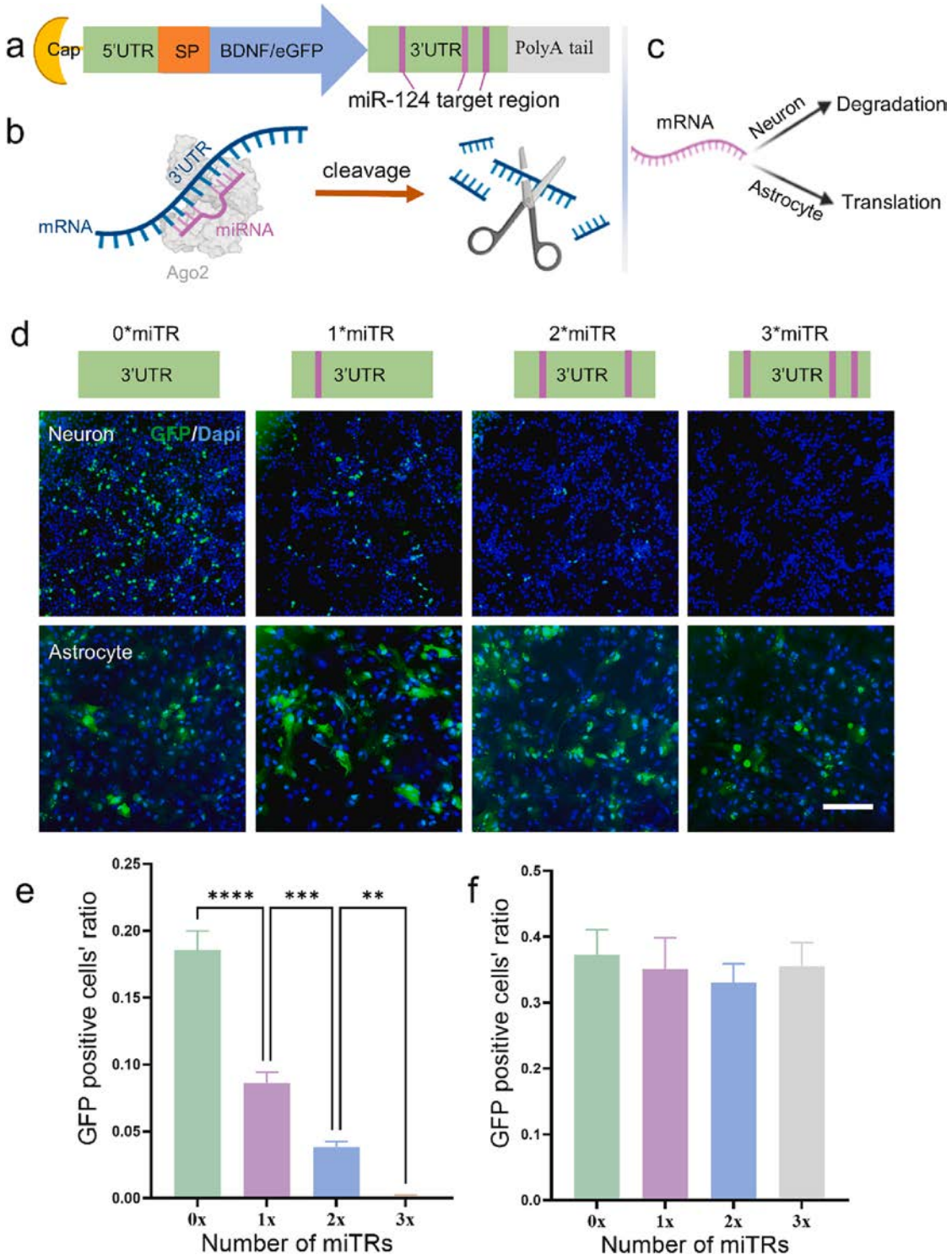

Fig. 4. Mrna engineering and modified in3′UTR. (a) Structure of mRNA with 3′UTR modification. (b) Mechanism illustrating mRNA degraded by miRNA when the target was inserted into the UTR. (c) Engineering mRNA could achieve neuron de-target delivery. (d) The GFP mRNA modified with 0–3 miRNA-target regions and delivered, showing the degradation in primary neurons and translation in primary astrocytes. (e) Bar chart of engineering GFP mRNA translation in primary neuron. (f) Bar chart of engineering GFP mRNA translation in primary astrocytes. miTR, miRNA translational target region. Scale bar = 200 μm. *p 0.05. (n = 3 biological repeats).

±2.2%, 25.1±2.7%, 33.1±1.7%, and 35.5±2.1%, respectively) (Fig. 4d and f). After the mRNA 3′UTR engineering, the BDNF mRNA nanoparticle would not trigger the mice seizure, monitored by camera for 24 h.

3.5. BDNF expression in vitro

BDNF protein expression was tested at three levels. First, the BDNF mRNA with a 6× His tag was transfected into 293T cells (i.e., cells with no intrinsic BDNF expression). The protein was expressed in 293T cells and could be stained with both anti-His and anti-BDNF antibodies. Immunofluorescent (IF) staining His tag (red) co-localized with BDNF protein (green) (Fig. 5a). Thus, BDNF mRNA correctly translated into protein. Second, BNDF mRNA could translate the protein of interest in astrocytes. Finally, we tested the ability of astrocytes to release BDNF protein. A *trans*-well model was established, with the upper layer being astrocytes and the lower layer being neurons (Fig. 5b). The quantity of BDNF released in the culture medium was measured by ELISA, and the activation of TrkB receptors in neurons was identified using IF staining. Neurons could be activated by the release of BDNF by transfected astrocytes. More specifically, the His tag was evident in nearly all neurons and p-TrkB (Y817) (green) was activated. In the absence of BDNF mRNA or in appearance of BDNF mRNA negative control (no cap and no polyA tail), astrocytes were unable to activate the neurons in the *trans*-well model (Figs. S6 and S7). Generally—and after three levels of testing—the BDNF mRNA could correctly translate into protein and efficiently activate the neurons.

3.6. BDNF release rate

BDNF protein was released with a Ca^{2+} trigger [36]. The vesicles for BDNF release were visualized by Flou-4 AM, which is a type of calcium indicator. Finally, 50 mM potassium chloride [37] was used to depolarize the astrocytes and trigger BDNF release. The whole process was completed in 15 s per once. The vesicles formed in the central soma and then moved to the cell membrane before released by exocytosis (Fig. 5c and Video 2). The release of BDNF in the culture medium primarily occurred during the first two days. Typically, the Object location tests are used on astrocyte released BDNF at a rate of 43.5±3.4 pg mL ^{1} day ^{1}. After PBAE treatment, the level of BDNF exocytosis was 36.6 ±3.4 pg mL ^{1} day ^{1} ($p > 0.05$). This result indicated that PBAE did not affect astrocyte exocytosis. As for BDNF mRNA (both 0 miRNA target region and 3 miRNA target regions), half of the total BDNF protein was released on the two days at 1226±43.82 pg mL ^{1} day ^{1}and 1233±99.8 pg mL ^{1} day ^{1}, respectively. BDNF mRNA transfected astrocytes had higher protein levels (approximately 15× relative to control); moreover, this BDNF protein release was maintained for 4 days (Fig. 5d).

3.7. BDNF protected neurons from aβ

Next, we tested the effect of BDNF-derived astrocytes on neurons. The viability of neurons was measured when exposed to β-amyloid 25–35 (aβ, AD's toxic agent) in the previously described *trans*-well

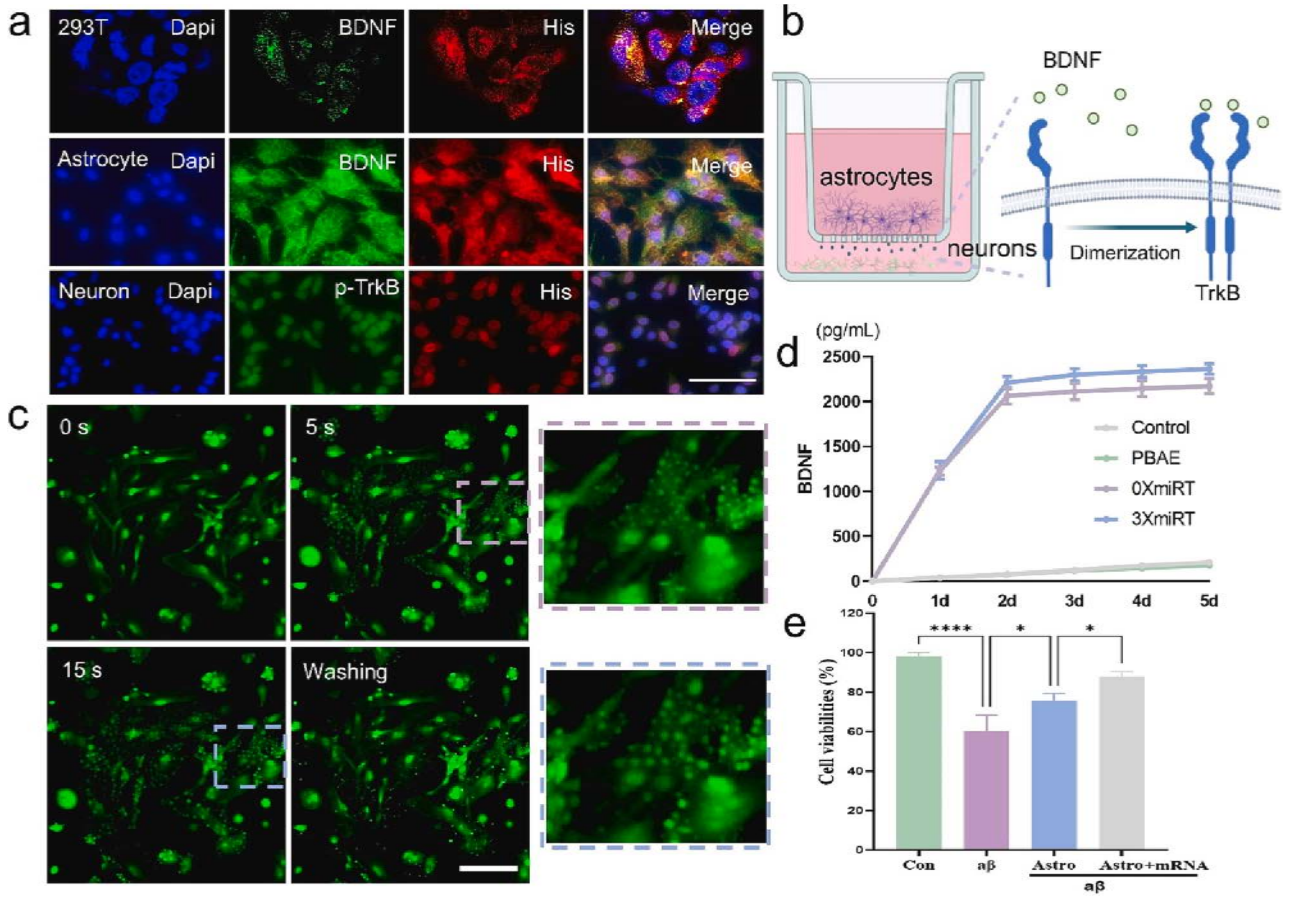

Fig. 5. BDNF mRNA expression and release rate. (a) BDNF mRNA expressed in 293 T and astrocytes (BDNF in Green and His tag in Red). Neuron was activated by released BDNF in a *trans*-well model (p-TrkB in Green and His in Red). (b) Trans-well model illustration, with the upper layer containing astrocytes with mRNA transfection and the lower layer containing neurons. The BDNF released from astrocytes could cross the membrane into the lower layer. (c) Visualization of BDNF vehicles released from the cells by calcium sensor. Scale bar = 200 μm. (d) Quantity of BDNF released by ELISA, tested within 5 days. (e) Neuronal viability with β-amyloid in the *trans*-well co-culture model. *p 0.05; ****p 0.0001; ns, $p > 0.05$ (n = 3 biological repeats).

model. When treated with aβ, the lowest cell viability was 60.3±4.7% when compared with control. When astrocytes were co-cultured with impaired neurons, the cell viability was enhanced to 75.7±2.0%. In addition, with assistance from BDNF, the cell viability was restored to 88.0±1.4% (Fig. 5e). As for neuronal proliferation, 5-ethynyl-2′-deoxyuridine (EdU)—a thymidine analog—was incorporated into newly synthesized DNA. An EdU assay indicated aβ-impaired neuron proliferation; more specifically, the percentage of EdU-positive cells went down from 48.2±5.2% to 26.7±4.0%. After co-culture with astrocytes or BDNF mRNA transfected astrocytes, neuronal proliferation was rescued to 34.5±1.2% and 45.1±4.2%, respectively (Fig. S8).

3.8. Ventricle injection and biocompatibility

The APP/PS1 *trans*-genetic mice (>9 months) were used as the AD model. For the future clinic application, a brain infusion catheter system was developed, which was like Ommaya reservoir for replacing intrathecal injection. It was inserted into the brain ventricle guided by a stereotaxic apparatus (Fig. S9a and b). Drug in the microliter amount was hard to accurately deliver into the ventricle, owing to the air bias (i.e., space between the syringe and tube). Given this, we tested several patterns of injecting. This included sealing by parafilm and filling mineral oil (Fig. S9). This resulted in 5 μL fluid injection, which was assisted by parafilm and mineral oil. The quantity of fluid was measured on the ventricular end. Using parafilm to seal the border of the tube solved the injection difficulties (No seal vs. Parafilm vs. Parafilm and Oil, 0.16±0.1 μL vs. 4.4±0.1 μL vs. 6.1±0.2 μL, respectively).

To test the mRNA/PBAE biosafety, nanoparticle was injected into the ventricle. After, H&E staining on major organ slices was used to estimate any obvious signs of damage (Fig. S10). There was no evident necrosis, inflammation, or edema in the organs.

3.9. BDNF improved behavior in vivo

After the catheter was implanted into the ventricles of aging mice, mice were allowed to recover for a month. After this recovery period, 5 continuous injections were administered every 5 days (Fig. 6a). Behavioral tests were then conducted, including 8-arm maze test, dark/light box, and object location test on day 65. Before the 8-arm maze test, food rewards were placed in 4 arms and the mice were trained for 5 days. AD mice showed better memory with treatment, with the low dose (1.5 μg mRNA) and high dose (3 μg mRNA) contributing to better maze-performing behavior. This was determined by total entrance times ranging from 15.3±0.9 in the control group to 8.5±1.0 in low dose group and 8.8±1.4 in the high dose group (p 0.05). The total entrance times of aging wild type mice was 5.5±0.65, and there was no significant statistical difference between low and high dose groups. Reference memory error (i.e., entrance into the wrong arm without food rewards) improved from 7±0.9 times (control) to 3.8 times (both low and high dose groups), and there was no significant statistical difference with wild type group (1.25±0.6 times) and mRNA treatment groups. In addition, working memory error (i.e., entrance into the same arm, excluding the first entrance) enhanced the behavior from 4.75±1.0 times (control) to 1.3±0.75 times (low dose), 0.5±0.3 times (high dose) and 0.25±0.25 times (wild type) (Fig. 6b and d).

Object location test was used to assess the mouse spatial memory skills. Based on the inherent exploring behavior of mice, mice generally spend longer time exploring a novel object. After BDNF treatment, mice recognized a familiar object, even when it was moved to a new location. As a result, they spent less time with the familiar object (old duration/new duration, WT vs. Con vs. Low dose vs. High dose, 1.34±0.19, 4.2 ±0.7, 1.7±0.1, and 1.3±0.1) (Fig. 6e and g).

Besides memory, anxiety was also explored using a light/dark box. When feeling anxious, mice prefer a dark environment rather than a light one. BDNF treatment had no effect on anxiety level (control vs. low dose vs. high dose, 120.4±9.5 s, 131.5±8.5 s, and 120.5±8.6 s). However, the wild type group showed higher exploration time in light box (191.8±14.1 s) (Fig. 6f and h).

The level of BDNF in CSF after low and high dose mRNA treatment could persist nearly half a month, from 2654±61.1 pg/mL (high dose) and 2136±137 pg/mL (low dose) on day 1 slowly decreased to 1591 ±99.5 pg/mL (high dose) and 1201±87.8 pg/mL (low dose) on day 15, respectively. The BDNF protein in wild type and control group was 1732 ±152.6 pg/mL and 905.9±33.9 pg/mL, respectively (Fig. S11). The BDNF mRNA may have an effect of positive feedback loop in brain, thereby triggering the endogenous BDNF expression.

3.10. BDNF activated downstream pathway in vivo

CA1 and CA3 regions in the hippocampus are known to be highly related to spatial memory [38]. Postsynaptic density protein 95 (PSD-95) has been shown to be involved in synaptic transmission and blocks ion-flux-independent long-term depression (LTD), which is a process that enhanced the connections between neurons to encode memory. This contributes to the mice's spatial memory [39]. After a month of BDNF mRNA treatment, BDNF activated its receptor TrkB and resulted in phosphorylation. After TrkB receptor activation, it modulated the synaptic plasticity by PI3-K/Akt pathway. Examination of brain slices indicated the p-TrkB (Y817) expression was highly related to BDNF mRNA dose in both CA3 and CA1 regions (Fig. 6c). Similarly, PSD95 expression was coincidental with p-TrkB (Fig. 6c). Thus, BDNF had a positive effect on its downstream pathway and PSD-95 expression.

BDNF also protected neurons from degradation. However, compared with the control group, the low and high dose groups did not show a significant decrease in FJB-positive cells (i.e., cells that are degraded) (Fig. S12). This may have resulted from either short-term treatment or a low rate of neural degradation.

4. Discussion

We have described here a BDNF mRNA delivery system for CNS application. The mRNA engineering by AI and miRNA target region achieved higher transcription and de-targeted neurons. Currently, targeted delivery of mRNA to liver, spleen, and lung have been achieved [40–42]. However, delivery of mRNA across the blood-brain barrier (BBB) remains challenging, even with specific modifications like peptides, adaptors, and/or antibodies [43]. With the development of catheter tubing and programming pump in hydrocephalus, an intrathecal injection could be easily achieved to allow nanoparticles crossing the BBB and be delivered into the CNS [44]. This study also modified the 3′UTR with neuron-specific miRNA complementary sequence. After endocytosis into the neurons, mRNA would be cleaved by the miRNA-124 guide. Apart from neurons, engineering mRNA was translated into protein in the cells with negligible amounts of miRNA-124.

AI has been involved in all parts of drug research and development, including design, screening and prediction [45,46]. In this study, we applied an AI algorithm to linearize the mRNA structure. This led to an increase in resulting protein expression by almost one-third. Moreover, AI-predicted and assisted protein drug design has been established only recently [47–49]. After the peptide or antibody was designed, the corresponding mRNA was synthesized and translated into the target protein with low cost and high efficiency. Thus, combining mRNA technology and AI would allow a shortening of the process from protein drug discovery to application.

Since its discovery in 1956, BDNF has good potential for the treatment of neurodegenerative diseases [50,51]. However, BDNF induces neuropathic pain and seizures when directly injected into the CNS [16,35]. The viral delivery of the BDNF gene—instead of the BDNF protein itself—was then developed. Nevertheless, the genotoxicity and immune clearance of the AAV delivery vehicle remained significant limitations [4,52].

At present, mRNA technology offers a way to achieve high level of

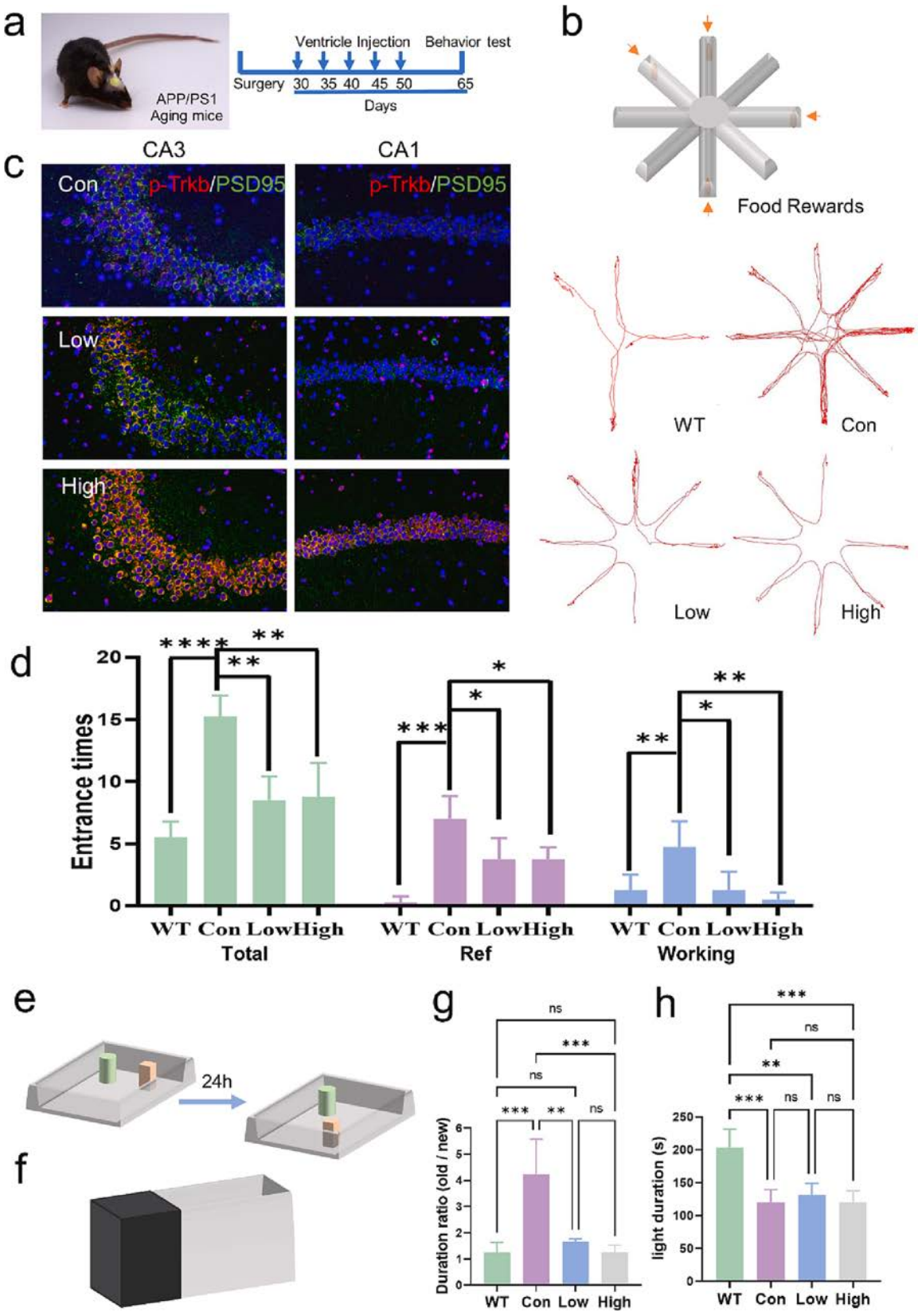

Fig. 6. BDNF mRNA delivery in a mouse model of AD. (a) Ventricle catheter system model in AD mice and treatment schedules. (b) Mice behavioral tests in 8-arm maze and their movement tracking. Arrows indicate food rewards. (c) Immunostaining of brain slices (p-Trkb in red and PSD 95 in green). Scale bar = 100 μm. (d) Bar charts of 8-arm maze results. (e, g) Object location test illustration and bar chart. Duration ratio is the time ratio of mice explored the old and new objects. (f, h) Light/dark box and bar charts. Light duration was the time that mice spent in the light zone. *p 0.05; **p 0.01; ***p 0.001; ****p 0.0001; and ns, $p > 0.05$ (n = 16 mice).

protein expression (e.g., 15× higher than normal astrocytes) and an achievable treatment approach. Also, the high expression of BDNF resulted in significant side effects, including neuronal excitotoxicity and symptomatic seizures. Some of these limitations were solved by 3′UTR modification to de-target the neuron for delivery, and it changed the BDNF secretion ways from neural autocrine to astrocytes' paracrine. Importantly, this modification pattern could achieve one or more specific cell types to de-target. Specifically, we successfully de-targeted neurons using miRNA-124. This approach could also achieve de-targeted astrocytes by using an astrocyte-specific miRNA. Similarly, a series of neuron- and astrocyte-specific miRNA sequences could be employed to deliver just to microglia. Promisingly, this 3′UTR pattern may be applicable to glioma treatment by delivering toxic protein into the glioma cells without affecting neuron.

The two different mRNA doses—1.5 μg and 3 μg—used in this study did not show a significant difference in behavioral tests. This phenomenon was similar to what was observed with previous COVID-19 mRNA vaccine. Moderna vaccine mRNA-1273 doses (250 μg, 100 μg and 25 μg) were used in the clinical trials [8]. Similarly, three BioNTech vaccine BNT162b2 doses (100 μg, 30 μg and 10 μg) were also tested in trials [7]. Both of these companies ultimately chose the lower doses of mRNA (100 μg in mRNA-1273 and 30 μg in BNT162b2) to market. These results indicated the similar phenomenon with our behavior tests results.

In conclusion, PBAE exhibit potential for use in CNS delivery. These polymers are easy to formulate with mRNA or DNA nanoparticles with a simple and quick approach. Based on this PBAE-mediated delivery, previous studies have shown tumor treatment [53], CAR-T [54], base editing [33], and stem cells therapy [55]. In this study, both PBAE-111 and 211 were selected for mRNA delivery in CNS. Both had good biocompatibility and high transfection rates. Importantly, these two polymers showed different application purposes. To this end, PBAE-111 allows for brain and spinal cord transfection using ventricular injection, thereby allowing for larger lesion areas to be targeted. PBAE-211 is another effective and focused local delivery agent and would be most useful for a focal lesion. Collectively, these two PBAEs would cover a great number of neurological and neurodegenerative diseases.

5. Conclusion

In this paper, we identified PBAE-111 as suitable for mRNA delivery into the CNS. We used an AI algorithm and 3′UTR modification to enhance the protein expression while also achieving de-target delivery to neuron. This approach enabled enhanced memory in a mouse model of AD. To summarize, this study developed a low-side-effect neurotrophic factor mRNA therapy for treating neurodegenerative diseases. Engineering mRNA drug provides a de-targeted delivery approach for treating neurological and neurodegenerative diseases by targeting specific cell types.

Declaration of Competing Interest

The authors declare that they have no known competing financial interests or personal relationships that could have appeared to influence the work reported in this paper.

Data availability

Data will be made available on request.

Acknowledgements

The work was partially supported by National Natural Science Foundation of China under Grant 82072020, Shanghai youth science and technology bright star program 20QA1401900, Shanghai Municipal Science and Technology Major Project 2018SHZDZX01, CAMS Innovation Fund for Medical Sciences (CIFMS, 2019-I2M-5-008), Shanghai Science and Technology Commission 21ZR1442200, Shanghai Pujiang Program (20PJ1410200), the ShanghaiTech University startup grant, and the Huashan Hospital startup grant.

Appendix A. Supplementary data

Supplementary data to this article can be found online at https://doi.org/10.1016/j.cej.2023.143152.

References

[1] L. Olson, A. Nordberg, H. Holst, L. Backman, T. Ebendal, I. Alafuzoff, K. Amberla, P. Hartvig, A. Herlitz, A. Lilja, H. Lundqvist, B. Långstrom, B. Meyerson, A. Persson, M. Viitanen, B. Winblad, Å. Seiger, Nerve growth factor affects 11C-nicotine binding, blood flow, EEG, and verbal episodic memory in an Alzheimer patient (case report), J Neural Transm Park Dis Dement Sect 4 (1) (1992) 79–95.

[2] M. Eriksdotter Jonhagen, A. Nordberg, K. Amberla, L. Backman, T. Ebendal, B. Meyerson, L. Olson, Å. Seiger, M. Shigeta, E. Theodorsson, M. Viitanen, B. Winblad, L.-O. Wahlund, Intracerebroventricular infusion of nerve growth factor in three patients with Alzheimer's disease, Dement Geriatr Cogn Disord 9 (5) (1998) 246–257.

[3] M.H. Tuszynski, L. Thal, M. Pay, D.P. Salmon, H.S. U, R. Bakay, P. Patel, A. Blesch, H.L. Vahlsing, G. Ho, G. Tong, S.G. Potkin, J. Fallon, L. Hansen, E.J. Mufson, J. H. Kordower, C. Gall, J. Conner, A phase 1 clinical trial of nerve growth factor gene therapy for Alzheimer disease, Nat Med 11 (5) (2005) 551–555.

[4] M.S. Rafii, M.H. Tuszynski, R.G. Thomas, D. Barba, J.B. Brewer, R.A. Rissman, J. Siffert, P.S. Aisen, Adeno-Associated Viral Vector (Serotype 2)-Nerve Growth Factor for Patients With Alzheimer Disease: A Randomized Clinical Trial, JAMA Neurol 75 (7) (2018) 834.

[5] T. Weber, Anti-AAV Antibodies in AAV Gene Therapy: Current Challenges and Possible Solutions, Front Immunol 12 (2021), 658399, https://doi.org/10.3389/fimmu.2021.658399.

[6] G.N. Nguyen, J.K. Everett, S. Kafle, A.M. Roche, H.E. Raymond, J. Leiby, C. Wood, C.A. Assenmacher, E.P. Merricks, C.T. Long, H.H. Kazazian, T.C. Nichols, F. D. Bushman, D.E. Sabatino, A long-term study of AAV gene therapy in dogs with hemophilia A identifies clonal expansions of transduced liver cells, Nat Biotechnol 39 (1) (2021) 47–55, https://doi.org/10.1038/s41587-020-0741-7.

[7] M.J. Mulligan, K.E. Lyke, N. Kitchin, J. Absalon, A. Gurtman, S. Lockhart, K. Neuzil, V. Raabe, R. Bailey, K.A. Swanson, P. Li, K. Koury, W. Kalina, D. Cooper, C. Fontes-Garfias, P.Y. Shi, O. Tureci, K.R. Tompkins, E.E. Walsh, R. Frenck, A. R. Falsey, P.R. Dormitzer, W.C. Gruber, U. Sahin, K.U. Jansen, Phase I/II study of COVID-19 RNA vaccine BNT162b1 in adults, Nature 586 (7830) (2020) 589–593, https://doi.org/10.1038/s41586-020-2639-4.

[8] L.A. Jackson, E.J. Anderson, N.G. Rouphael, P.C. Roberts, M. Makhene, R.N. Coler, M.P. McCullough, J.D. Chappell, M.R. Denison, L.J. Stevens, A.J. Pruijssers, A. McDermott, B. Flach, N.A. Doria-Rose, K.S. Corbett, K.M. Morabito, S. O'Dell, S.D. Schmidt, P.A. Swanson, 2nd, M. Padilla, J.R. Mascola, K.M. Neuzil, H. Bennett, W. Sun, E. Peters, M. Makowski, J. Albert, K. Cross, W. Buchanan, R. Pikaart-Tautges, J.E. Ledgerwood, B.S. Graham, J.H. Beigel, R.N.A.S.G. m, An mRNA Vaccine against SARS-CoV-2 - Preliminary Report, N Engl J Med 383(20) (2020) 1920-1931. doi: 10.1056/NEJMoa2022483.

[9] L.C. Vu, L. Piccenna, P. Kwan, T.J. O'Brien, New-onset epilepsy in the elderly, Br J Clin Pharmacol 84 (10) (2018) 2208–2217, https://doi.org/10.1111/bcp.13653.

[10] S. Schildge, C. Bohrer, K. Beck, C. Schachtrup, Isolation and culture of mouse cortical astrocytes, J Vis Exp 71 (2013), https://doi.org/10.3791/50079.

[11] A.R. Mendelsohn, J.W. Larrick, Inflammation, Stem Cells, and the Aging Hypothalamus, Rejuvenation Res 20 (4) (2017) 346–349, https://doi.org/10.1089/rej.2017.2002.

[12] R.J. Kotloski, J. Dowding, B.P. Hermann, T.P. Sutula, Epilepsy and aging, Handb Clin Neurol 167 (2019) 455–475, https://doi.org/10.1016/B978-0-12-804766-8.00025-X.

[13] M. Roy-O'Reilly, L.D. McCullough, Age and Sex Are Critical Factors in Ischemic Stroke Pathology, Endocrinology 159 (8) (2018) 3120–3131, https://doi.org/10.1210/en.2018-00465.

[14] M.E. Davis, Epidemiology and Overview of Gliomas, Semin Oncol Nurs 34 (5) (2018) 420–429, https://doi.org/10.1016/j.soncn.2018.10.001.

[15] S.D. Croll, C. Suri, D.L. Compton, M.V. Simmons, G.D. Yancopoulos, R.M. Lindsay, S.J. Wiegand, J.S. Rudge, H.E. Scharfman, Brain-derived neurotrophic factor transgenic mice exhibit passive avoidance deficits, increased seizure severity and in vitro hyperexcitability in the hippocampus and entorhinal cortex, Neuroscience 93 (4) (1999) 1491–1506, https://doi.org/10.1016/s0306-4522(99)00296-1.

[16] L. Iughetti, L. Lucaccioni, F. Fugetto, B. Predieri, A. Berardi, F. Ferrari, Brain-derived neurotrophic factor and epilepsy: a systematic review, Neuropeptides 72 (2018) 23–29, https://doi.org/10.1016/j.npep.2018.09.005.

[17] B. de Pins, C. Cifuentes-Diaz, A.T. Farah, L. Lopez-Molina, E. Montalban, A. Sancho-Balsells, A. Lopez, S. Gines, J.M. Delgado-Garcia, J. Alberch, A. Gruart, J.A. Girault, A. Giralt, Conditional BDNF Delivery from Astrocytes Rescues Memory Deficits, Spine Density, and Synaptic Properties in the 5xFAD Mouse Model of Alzheimer Disease, J Neurosci 39 (13) (2019) 2441–2458, https://doi.org/10.1523/JNEUROSCI.2121-18.2019.

[18] F. Wada, T. Yamamoto, T. Kobayashi, K. Tachibana, K.R. Ito, M. Hamasaki, Y. Kayaba, C. Terada, A. Yamayoshi, S. Obika, M. Harada-Shiba, Drug discovery and development scheme for liver-targeting bridged nucleic acid antisense

oligonucleotides, Mol Ther Nucleic Acids 26 (2021) 957–969, https://doi.org/10.1016/j.omtn.2021.10.008.
[19] L. Miao, L. Li, Y. Huang, D. Delcassian, J. Chahal, J. Han, Y. Shi, K. Sadtler, W. Gao, J. Lin, J.C. Doloff, R. Langer, D.G. Anderson, Delivery of mRNA vaccines with heterocyclic lipids increases anti-tumor efficacy by STING-mediated immune cell activation, Nat Biotechnol 37 (10) (2019) 1174–1185, https://doi.org/10.1038/s41587-019-0247-3.
[20] M. Qiu, Z. Glass, J. Chen, M. Haas, X. Jin, X. Zhao, X. Rui, Z. Ye, Y. Li, F. Zhang, Q. Xu, Lipid nanoparticle-mediated codelivery of Cas9 mRNA and single-guide RNA achieves liver-specific in vivo genome editing of Angptl3, Proc Natl Acad Sci U S A 118 (10) (2021), https://doi.org/10.1073/pnas.2020401118.
[21] S.A. Dilliard, Q. Cheng, D.J. Siegwart, On the mechanism of tissue-specific mRNA delivery by selective organ targeting nanoparticles, Proc Natl Acad Sci U S A 118 (52) (2021), https://doi.org/10.1073/pnas.2109256118.
[22] J. Krol, I. Loedige, W. Filipowicz, The widespread regulation of microRNA biogenesis, function and decay, Nat Rev Genet 11 (9) (2010) 597–610, https://doi.org/10.1038/nrg2843.
[23] P. Gaspar, G. Moura, M.A. Santos, J.L. Oliveira, mRNA secondary structure optimization using a correlated stem-loop prediction, Nucleic Acids Res 41 (6) (2013) e73.
[24] J.J. Cannone, S. Subramanian, M.N. Schnare, J.R. Collett, L.M. D'Souza, Y. Du, B. Feng, N. Lin, L.V. Madabusi, K.M. Muller, N. Pande, Z. Shang, N. Yu, R.R. Gutell, The comparative RNA web (CRW) site: an online database of comparative sequence and structure information for ribosomal, intron, and other RNAs, BMC Bioinformatics 3 (2002) 2, https://doi.org/10.1186/1471-2105-3-2.
[25] H. Zhang, L. Zhang, A. Lin, C. Xu, Z. Li, K. Liu, B. Liu, X.-T. Ma, F. Zhao, W. Yao, H. Li, D.H. Mathews, Y. Zhang, L. Huang, Algorithm for Optimized mRNA Design Improves Stability and Immunogenicity (2020).
[26] N. Chaudhary, D. Weissman, K.A. Whitehead, mRNA vaccines for infectious diseases: principles, delivery and clinical translation, Nat Rev Drug Discov 20 (11) (2021) 817–838, https://doi.org/10.1038/s41573-021-00283-5.
[27] J.J. Green, G.T. Zugates, R. Langer, D.G. Anderson, Poly(beta-amino esters): procedures for synthesis and gene delivery, Methods Mol Biol 480 (2009) 53–63, https://doi.org/10.1007/978-1-59745-429-2_4.
[28] F. Yang, J.J. Green, T. Dinio, L. Keung, S.W. Cho, H. Park, R. Langer, D. G. Anderson, Gene delivery to human adult and embryonic cell-derived stem cells using biodegradable nanoparticulate polymeric vectors, Gene Ther 16 (4) (2009) 533–546, https://doi.org/10.1038/gt.2008.182.
[29] J.J. Green, R. Langer, D.G. Anderson, A combinatorial polymer library approach yields insight into nonviral gene delivery, Acc Chem Res 41 (6) (2008) 749–759, https://doi.org/10.1021/ar7002336.
[30] Y. Liu, Y. Li, D. Keskin, L. Shi, Poly(beta-Amino Esters): Synthesis, Formulations, and Their Biomedical Applications, Adv Healthc Mater 8 (2) (2019) e1801359.
[31] J.M. Richner, S. Himansu, K.A. Dowd, S.L. Butler, V. Salazar, J.M. Fox, J. G. Julander, W.W. Tang, S. Shresta, T.C. Pierson, G. Ciaramella, M.S. Diamond, Modified mRNA Vaccines Protect against Zika Virus Infection, Cell 168 (6) (2017) 1114–1125.e10.
[32] M. Keeney, L. Deveza, F. Yang, Programming stem cells for therapeutic angiogenesis using biodegradable polymeric nanoparticles, J Vis Exp (79) (2013) e50736.
[33] Q. Chen, L. Su, X. He, J. Li, Y. Cao, Q. Wu, J. Qin, Z. He, X. Huang, H. Yang, J. Li, Poly(beta-amino ester)-Based Nanoparticles Enable Nonviral Delivery of Base Editors for Targeted Tumor Gene Editing, Biomacromolecules 23 (5) (2022) 2116–2125.
[34] S. Kaech, G. Banker, Culturing hippocampal neurons, Nat Protoc 1 (5) (2006) 2406–2415, https://doi.org/10.1038/nprot.2006.356.
[35] D.K. Binder, S.D. Croll, C.M. Gall, H.E. Scharfman, BDNF and epilepsy: too much of a good thing? Trends Neurosci 24 (1) (2001) 47–53, https://doi.org/10.1016/s0166-2236(00)01682-9.
[36] J.-H. Liu, M. Zhang, Q. Wang, D.-Y. Wu, W. Jie, N.-Y. Hu, J.-Z. Lan, K. Zeng, S.-J. Li, X.-W. Li, J.-M. Yang, T.-M. Gao, Distinct roles of astroglia and neurons in synaptic plasticity and memory, Mol Psychiatry 27 (2) (2022) 873–885.
[37] O.L. Barreto-Chang, R.E. Dolmetsch, Calcium imaging of cortical neurons using Fura-2 AM, J Vis Exp (23) (2009), https://doi.org/10.3791/1067.
[38] I. Soltesz, A. Losonczy, CA1 pyramidal cell diversity enabling parallel information processing in the hippocampus, Nat Neurosci 21 (4) (2018) 484–493, https://doi.org/10.1038/s41593-018-0118-0.
[39] K. Dore, Z. Carrico, S. Alfonso, M. Marino, K. Koymans, H.W. Kessels, R. Malinow, PSD-95 protects synapses from beta-amyloid, Cell Rep 35 (9) (2021), 109194, https://doi.org/10.1016/j.celrep.2021.109194.
[40] Q. Cheng, T. Wei, L. Farbiak, L.T. Johnson, S.A. Dilliard, D.J. Siegwart, Selective organ targeting (SORT) nanoparticles for tissue-specific mRNA delivery and CRISPR-Cas gene editing, Nat Nanotechnol 15 (4) (2020) 313–320, https://doi.org/10.1038/s41565-020-0669-6.
[41] S. Liu, Q. Cheng, T. Wei, X. Yu, L.T. Johnson, L. Farbiak, D.J. Siegwart, Membrane-destabilizing ionizable phospholipids for organ-selective mRNA delivery and CRISPR-Cas gene editing, Nat Mater 20 (5) (2021) 701–710, https://doi.org/10.1038/s41563-020-00886-0.
[42] J.C. Kaczmarek, A.K. Patel, L.H. Rhym, U.C. Palmiero, B. Bhat, M.W. Heartlein, F. DeRosa, D.G. Anderson, Systemic delivery of mRNA and DNA to the lung using polymer-lipid nanoparticles, Biomaterials 275 (2021), 120966, https://doi.org/10.1016/j.biomaterials.2021.120966.
[43] G.C. Terstappen, A.H. Meyer, R.D. Bell, W. Zhang, Strategies for delivering therapeutics across the blood-brain barrier, Nat Rev Drug Discov 20 (5) (2021) 362–383, https://doi.org/10.1038/s41573-021-00139-y.
[44] P. Van Damme, P. Tilkin, K.J. Mercer, J. Terryn, A. D'Hondt, N. Herne, T. Tousseyn, K.G. Claeys, D.R. Thal, O. Zachrisson, P. Almqvist, B. Nuttin, M. Jerling, F. Bernadotte, A. Haegerstrand, W. Robberecht, Intracerebroventricular delivery of vascular endothelial growth factor in patients with amyotrophic lateral sclerosis, a phase I study, Brain Commun 2 (2) (2020) fcaa160, https://doi.org/10.1093/braincomms/fcaa160.
[45] A. Sharma, T. Virmani, V. Pathak, A. Sharma, K. Pathak, G. Kumar, D. Pathak, U. A. Ashfaq, Artificial Intelligence-Based Data-Driven Strategy to Accelerate Research, Development, and Clinical Trials of COVID Vaccine, Biomed Res Int 2022 (2022) 1–16.
[46] X. Yang, Y. Wang, R. Byrne, G. Schneider, S. Yang, Concepts of Artificial Intelligence for Computer-Assisted Drug Discovery, Chem Rev 119 (18) (2019) 10520–10594, https://doi.org/10.1021/acs.chemrev.8b00728.
[47] J. Jumper, R. Evans, A. Pritzel, T. Green, M. Figurnov, O. Ronneberger, K. Tunyasuvunakool, R. Bates, A. Zidek, A. Potapenko, A. Bridgland, C. Meyer, S.A. A. Kohl, A.J. Ballard, A. Cowie, B. Romera-Paredes, S. Nikolov, R. Jain, J. Adler, T. Back, S. Petersen, D. Reiman, E. Clancy, M. Zielinski, M. Steinegger, M. Pacholska, T. Berghammer, S. Bodenstein, D. Silver, O. Vinyals, A.W. Senior, K. Kavukcuoglu, P. Kohli, D. Hassabis, Highly accurate protein structure prediction with AlphaFold, Nature 596 (7873) (2021) 583–589, https://doi.org/10.1038/s41586-021-03819-2.
[48] M. Baek, F. DiMaio, I. Anishchenko, J. Dauparas, S. Ovchinnikov, G.R. Lee, J. Wang, Q. Cong, L.N. Kinch, R.D. Schaeffer, C. Millan, H. Park, C. Adams, C. R. Glassman, A. DeGiovanni, J.H. Pereira, A.V. Rodrigues, A.A. van Dijk, A. C. Ebrecht, D.J. Opperman, T. Sagmeister, C. Buhlheller, T. Pavkov-Keller, M. K. Rathinaswamy, U. Dalwadi, C.K. Yip, J.E. Burke, K.C. Garcia, N.V. Grishin, P. D. Adams, R.J. Read, D. Baker, Accurate prediction of protein structures and interactions using a three-track neural network, Science 373 (6557) (2021) 871–876, https://doi.org/10.1126/science.abj8754.
[49] L. Cao, B. Coventry, I. Goreshnik, B. Huang, J.S. Park, K.M. Jude, I. Markovic, R. U. Kadam, K.H.G. Verschueren, K. Verstraete, S.T.R. Walsh, N. Bennett, A. Phal, A. Yang, L. Kozodoy, M. DeWitt, L. Picton, L. Miller, E.M. Strauch, N.D. DeBouver, A. Pires, A.K. Bera, S. Halabiya, B. Hammerson, W. Yang, S. Bernard, L. Stewart, I. A. Wilson, H. Ruohola-Baker, J. Schlessinger, S. Lee, S.N. Savvides, K.C. Garcia, D. Baker, Design of protein binding proteins from target structure alone, Nature (2022), https://doi.org/10.1038/s41586-022-04654-9.
[50] S. Cohen, R. Levi-Montalcini, A Nerve Growth-Stimulating Factor Isolated from Snake Venom, Proc Natl Acad Sci U S A 42 (9) (1956) 571–574, https://doi.org/10.1073/pnas.42.9.571.
[51] R. Levi-Montalcini, S. Cohen, In Vitro and in Vivo Effects of a Nerve Growth-Stimulating Agent Isolated from Snake Venom, Proc Natl Acad Sci U S A 42 (9) (1956) 695–699, https://doi.org/10.1073/pnas.42.9.695.
[52] F. Mingozzi, K.A. High, Overcoming the Host Immune Response to Adeno-Associated Virus Gene Delivery Vectors: The Race Between Clearance, Tolerance, Neutralization, and Escape, Annu Rev Virol 4 (1) (2017) 511–534, https://doi.org/10.1146/annurev-virology-101416-041936.
[53] A. Mangraviti, S.Y. Tzeng, K.L. Kozielski, Y. Wang, Y. Jin, D. Gullotti, M. Pedone, N. Buaron, A. Liu, D.R. Wilson, S.K. Hansen, F.J. Rodriguez, G.D. Gao, F. DiMeco, H. Brem, A. Olivi, B. Tyler, J.J. Green, Polymeric nanoparticles for nonviral gene therapy extend brain tumor survival in vivo, ACS Nano 9 (2) (2015) 1236–1249, https://doi.org/10.1021/nn504905q.
[54] N.N. Parayath, S.B. Stephan, A.L. Koehne, P.S. Nelson, M.T. Stephan, In vitro-transcribed antigen receptor mRNA nanocarriers for transient expression in circulating T cells in vivo, Nat Commun 11 (1) (2020) 6080, https://doi.org/10.1038/s41467-020-19486-2.
[55] X. Jiang, S. Fitch, C. Wang, C. Wilson, J. Li, G.A. Grant, F. Yang, Nanoparticle engineered TRAIL-overexpressing adipose-derived stem cells target and eradicate glioblastoma via intracranial delivery, Proc Natl Acad Sci U S A 113 (48) (2016) 13857–13862, https://doi.org/10.1073/pnas.1615396113.